Supporting Information

catchyFOAM: Euler-Euler CFD simulation of fluidized bed reactors with microkinetic modeling of gas phase and catalytic surface chemistry

Laurien A. Vandewalle[1]

Guy B. Marin[1], Kevin M. Van Geem[1]*

[1]Ghent University, Laboratory for Chemical Technology, Technologiepark 125, 9052 Gent, Belgium.

*Corresponding author: Technologiepark 125, 9052 Gent, Belgium; Kevin.VanGeem@UGent.be

CONTENTS

SI-1. CALCULATION OF THERMODYNAMIC AND TRANSPORT PROPERTIES

The NASA 7-coefficient polynomial parameterization is used to compute the reference-state thermodynamic properties of the individual gas species.

$$c_{p,g,k}(T_g) = \left(a_{0,k} + a_{1,k}T_g + a_{2,k}T_g{}^2 + a_{3,k}T_g{}^3 + a_{4,k}T_g{}^4\right)\frac{R}{M_k} \tag{SI-1}$$

$$h_{g,k}(T_g) = \left(a_{0,k} + \frac{a_{1,k}}{2}T_g + \frac{a_{2,k}}{3}T_g{}^2 + \frac{a_{3,k}}{4}T_g{}^3 + \frac{a_{4,k}}{5}T_g{}^4 + \frac{a_{5,k}}{T_g}\right)\frac{RT_g}{M_k} \tag{SI-2}$$

The gas phase heat capacity and sensible enthalpy are calculated from these species-specific properties using the following mixing rules:

$$c_{p,g}(T_g) = \sum_{k=1}^{n_g} c_{p,g,k}Y_k \tag{SI-3}$$

$$h_g(T_g) = \sum_{k=1}^{n_g} \left(h_{g,k}(T_g) - h_k^{298}\right)Y_k \tag{SI-4}$$

After solution of the energy equation, an iterative procedure is used to solve eqn. (SI-4) for temperature. For the solid phase, a constant heat capacity is assumed, and the enthalpy is simply calculated as the product of this heat capacity with temperature, allowing an easy calculation of the solid phase temperature after solution of the solid phase energy equation.

$$h_s = c_{p,s}T_s \tag{SI-5}$$

Note that in reality, the solid phase heat capacity is temperature dependent, which may affect the results in case there are large temperature gradients. This has been ignored in the present study, mainly because there is little information about the solid phase heat capacities of the used catalysts, let alone their temperature dependence. However, when this information would be known, it is straightforward to include the temperature dependence of the solid phase heat capacity in the code for future studies.

The gas species viscosity and thermal conductivity are calculated using a polynomial fit as a function of the logarithm of temperature, rather than the complex kinetic gas theory expressions. The coefficients, $b_{i,k}$ and $d_{i,k}$, of these polynomials are calculated from Lennard-Jones parameters by Cantera during the conversion of the Cantera input file into OpenFOAM format.

$$\ln(\mu_{g,k}) = \sum_{i=1}^{8} b_{i,k} \ln(T_g)^{i-1} \tag{SI-6}$$

$$\ln(\lambda_{g,k}) = \sum_{i=1}^{8} d_{i,k} \ln(T_g)^{i-1} \tag{SI-7}$$

In OpenFOAM, the mixture properties are calculated by considering a pseudo-species, characterized by the mixture's mass-weighted average polynomial coefficients:

$$\nu_g = \frac{\mu_g}{\rho_g}, \quad \ln(\mu_g) = \sum_{i=1}^{8} \left(\sum_{k=1}^{n_g} b_{i,k} Y_k \right) \ln(T_g)^{i-1} \tag{SI-8}$$

$$\ln(\lambda_g) = \sum_{i=1}^{8} \left(\sum_{k=1}^{n_g} d_{i,k} Y_k \right) \ln(T_g)^{i-1} \tag{SI-9}$$

Note that these expressions are different from the kinetic gas theory mixing rule by Wilke [1].

No Stefan-Maxwell diffusion coefficients are used. Instead, the individual species' diffusivities are calculated from the species kinematic viscosity and the Schmidt number, which is set to one. Hence:

$$D_{g,k} = \frac{\mu_{g,k}}{\rho_g} \tag{SI-10}$$

SI-2. CATALYTIC MICROKINETIC MODEL

A microkinetic model, including catalyst descriptors, has been developed at the LCT to account for the heterogeneously catalyzed reaction steps. In the past decade, the model was shown to be applicable for a variety of catalysts (Li/MgO, Sn-Li/MgO, Sr/La$_2$O$_3$, LaSr/CaO, Na-Mn-W/SiO$_2$) [2–5]. The microkinetic model and its kinetic parameters are described in detail in previous work [3,4]. Only a summary is given below.

Table SI 1: Catalytic elementary steps considered in the detailed microkinetic OCM models used in this work. Kinetic parameters can be found in the work of Kechagiopoulos et al. [3] and Alexiadis et al. [4].

Adsorption steps	Eley-Rideal steps	Surface reaction steps
1) $O_2 + 2^* \leftrightarrow 2O^*$	8) $CH_4 + O^* \leftrightarrow CH_3\bullet + OH^*$	20) $2OH^* \leftrightarrow H_2O^* + O^*$
2) $H_2O^* \leftrightarrow H_2O + ^*$	9) $C_2H_4 + O^* \leftrightarrow C_2H_3\bullet + OH^*$	21) $CH_3O^* + O^* \leftrightarrow CH_2O^* + OH^*$
3) $CH_3\bullet + O^* \leftrightarrow CH_3O^*$	10) $C_2H_6 + O^* \leftrightarrow C_2H_5\bullet + OH^*$	22) $CH_2O^* + O^* \leftrightarrow HCO^* + OH^*$
4) $CO + ^* \leftrightarrow CO^*$	11) $C_2H_5\bullet + O^* \leftrightarrow C_2H_4 + OH^*$	23) $CHO^* + O^* \leftrightarrow CO^* + OH^*$
5) $CO_2 + ^* \leftrightarrow CO_2^*$	12) $CH_3O\bullet + O^* \leftrightarrow CH_2O + OH^*$	24) $CO^* + O^* \leftrightarrow CO_2^* + ^*$
6) $C_2H_4 + O^* \leftrightarrow C_2H_4O^*$	13) $CH_2O + O^* \leftrightarrow CHO\bullet + OH^*$	25) $C_2H_4O^* + O^* \leftrightarrow C_2H_3O^* + OH^*$
7) $HO_2\bullet + ^* \leftrightarrow OH\bullet + O^*$	14) $CHO\bullet + O^* \leftrightarrow CO + OH^*$	26) $C_2H_3O^* + O^* \leftrightarrow CH_2O^* + HCO^*$
	15) $H_2 + O^* \leftrightarrow H\bullet + OH^*$	
	16) $H_2O_2 + O^* \leftrightarrow HO_2\bullet + OH^*$	
	17) $OH\bullet + O^* \leftrightarrow O\bullet + OH^*$	
	18) $H_2O + O^* \leftrightarrow OH\bullet + OH^*$	
	19) $HO_2\bullet + O^* \leftrightarrow O_2 + OH^*$	

*: surface active site

•: gas-phase radical species

The 26 elementary steps on the catalyst surface considered in the microkinetic model of Alexiadis et al. [4] are shown in Table SI 1. The depicted catalytic steps can be classified into three types, that is, adsorption steps, Eley–Rideal reactions, and surface reactions. The catalytic network considers methane activation on the catalyst surface by the dissociative adsorption of oxygen

(step 1), hydrogen abstraction from methane (step 8), and regeneration of the active site (step 20 and 2). Methyl radicals couple in the gas phase to form ethane, which can be dehydrogenated into ethylene. However, methyl radicals can also be oxidized towards undesired carbon oxides, CO and CO_2. The latter is generated in the network through three possible reaction pathways: oxidation of the methyl radical followed by a series of hydrogen abstractions from methoxy species on the surface (steps 3, 21-24, 5), heterogeneous oxidation of ethylene followed by a hydrogen abstraction and C-C bond cleavage (steps 6, 25-26), and hydrogen abstraction from ethane and ethylene (steps 9-10) leading to radicals that are oxidized to CO_2 in the gas phase [4].

Microkinetic model parameters are classified into kinetic and catalyst descriptors. While the former are exclusively related to the reaction kinetics, independent of the catalyst used, the latter specifically account for the physical and chemical catalyst properties. The main advantage of incorporating catalyst descriptors into the microkinetic model for OCM is that the developed model is capable of quantifying trends between catalyst activity and selectivity on the one hand and properties on the other hand. As a result, such a model allows addressing which catalyst descriptors and, hence, corresponding properties are the most relevant for the improvement of catalytic performance.

Via thermodynamic relationships between surface reaction enthalpies and analogous gas-phase reactions, the reaction enthalpies for various elementary steps can be expressed as a function of a limited number of unknown descriptor values, which can then be obtained, for example, by regression. Furthermore, collision theory is used to calculate the pre-exponential factors of all steps involving the collision of a molecule on the catalyst surface.

All adsorption steps are considered to be non-activated. The Eley–Rideal are grouped into a single reaction family, while the surface reaction steps are subdivided into four reaction families,

accounting for H-atom abstraction, recombination of hydroxyls, catalytic oxidation of CO, and C–C bond scission. Each reaction family has a specific set of the Polanyi parameters α and E0, for which values are taken from literature [6–8].

Table SI 2: Overview of catalyst descriptors.

	4% Sn-2%Li /MgO [4]	1%Sr/La$_2$O$_3$ [4]	4%Sr-40%La /SiC
Specific surface area [m^2/kg]	2500	2500	6200
Density [kg/m^3]	2300	2300	2950
Porosity [-]	0.27	0.27	0.27
D1: Reaction enthalpy hydrogen abstraction from CH$_4$ [kJ/mol]	56.6	44.4	45
D2: Chemisorption heat of O$_2$ [kJ/mol]	60.5	119.5	90
D3: Chemisorption heat of CH$_2$O [kJ/mol]		123.1	
D4: Chemisorption heat of HCO [kJ/mol]		141.1	
D5: Chemisorption heat of CO [kJ/mol]		74.4	
D6: Chemisorption heat of CO$_2$ [kJ/mol]		87	
D7: Chemisorption heat of H$_2$O [kJ/mol]		34.8	
D8: Chemisorption heat of C$_2$H$_4$O [kJ/mol]		42.4	
D9: Chemisorption heat of C$_2$H$_3$O [kJ/mol]		92.6	
D10: Initial sticking probability of O$_2$ [-]		0.56	
D11: Initial sticking probability of CH$_3$ [-]	6.22 10^{-5}	6.49 10^{-4}	2.5 10^{-5}
D12: Initial sticking probability of CO [-]		5.66 10^{-5}	
D13: Initial sticking probability of CO$_2$ [-]		1.54 10^{-2}	
D14: Initial sticking probability of H$_2$O [-]		7.65 10^{-2}	
D15: Initial sticking probability of C$_2$H$_4$ [-]		5.48 10^{-5}	2.5 10^{-4}
D16: Density of active sites [mol/m^2]	1.33 10^{-6}	9.84 10^{-6}	3.9 10^{-6}

Table SI 2 gives an overview of the catalyst descriptor estimates as obtained by regression in the work of Alexiadis et al. [4,5,9]. The microkinetic model for the catalyst was hereby implemented

in a 1D heterogeneous PFR model, while simultaneously using the kinetic mechanism by Chen et al. [10] for the gas phase. This gas phase mechanism is only validated for a narrow range of typical OCM operating conditions, which does not cover the wide range of conditions studied in this work. The last column in Table SI 2 shows the descriptor values for the 4%Sr-40%La/SiC catalyst that is used in GSVR. The values of the catalyst descriptors are not published yet. They were obtained by comparison of packed bed experimental measurements with 1D pseudo-homogeneous PFR simulations, using the kinetic mechanism by Stagni et al. [11] for the gas phase.

SI-2.1. *NOTES ON OPTIMAL TEMPERATURE WINDOW*

An optimal temperature window for maximizing the C_2 selectivity is often reported in literature [12–14]. For a given catalyst (hence, kinetic model), this optimal temperature in terms of C_2 selectivity depends on operating conditions, more specifically, the $CH_4:O_2$ ratio, dilution, catalyst porosity and bed voidage. To investigate if an optimal temperature exists for the kinetics used in the present work, isothermal pseudo-homogeneous plug flow reactor simulations were performed in the temperature range 650-1100 °C, and this for operating conditions resembling those presented in §4.2.3 of the manuscript: $\varepsilon_s = 0.2$, $CH_4:O_2=4$, 80% N_2, $\varepsilon_p = 0.27$.

The corresponding C_2 selectivities were evaluated at constant CH_4 conversion, resulting in Figure SI-1. As can be seen in Figure SI-1a, the optimum temperature window shifts to higher temperatures with increasing CH_4 conversion. In Figure 13c of the manuscript, the C_2 selectivity flattens, because along this curve both the temperature in the reactor and the CH_4 conversion increase simultaneously. This is illustrated by the dashed grey line in Figure SI-1a. This grey line indicates that between 1000 K and 1200 K, it is indeed possible to have a constant C_2 selectivity if CH_4 conversion increases simultaneously with temperature. Note that for the higher values of

8

X_{CH4} in Figure SI-1a, it seems as if the C_2 selectivity keeps rising with increasing temperature. In reality however, degradation of the catalyst at higher temperatures will result in a drop of selectivity, which is not taken into account in the model.

Figure SI-1b shows a more detailed breakdown of the product selectivities for a fixed CH_4 conversion of 2.5 %. At higher temperatures than the optimum temperature for C_2 selectivity, not only C_2 selectivity drops, but also the selectivities towards CO and CO_2 drop. This is somehow compensated by a significant increase of CH_3 radicals in the product stream.
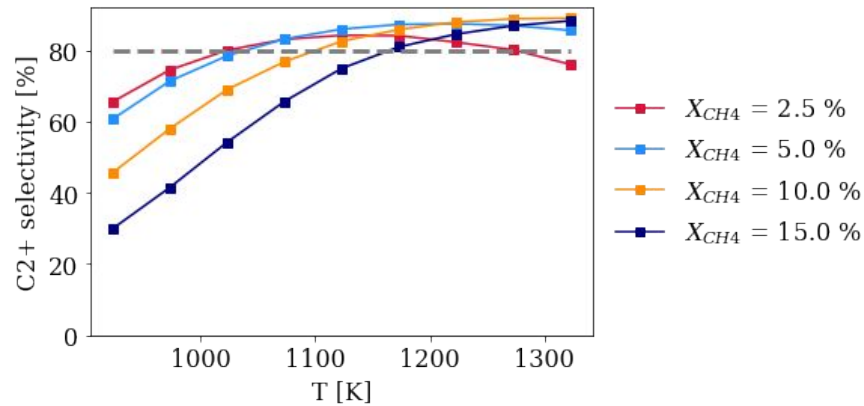
p
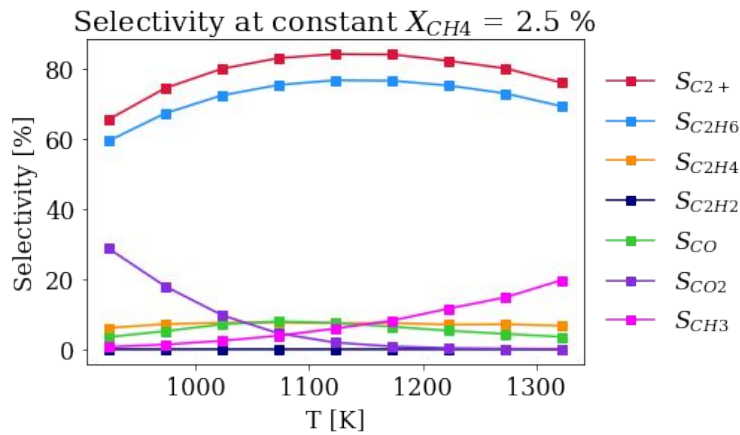
(b)

Figure SI 1: Product selectivity calculated using isothermal pseudo-homogeneous plug flow reactor simulations (operating conditions: $\varepsilon_s = 0.2$, CH_4:O_2=4, 80% N_2, $\varepsilon_p = 0.27$). The PFR equations are integrated up to the reactor length corresponding to the specified CH_4 conversion. (a) C_2 selectivity for varying CH_4 conversion, (b) selectivity towards selected species for fixed X_{CH4} =2.5 %.

As the reviewer mentions, at low temperatures, deep oxidation reactions are responsible for the lower C_2 selectivities, since they have a lower activation energy than the desired coupling reaction [12–14]. However, we believe there exists some controversy in literature about the drop in C_2 selectivity at higher temperatures. Indeed, this is often referred to as being due to reforming reactions in the gas phase but it is never actually rigorously proven. In literature, several works have reported the decrease in C_2 selectivity at higher temperatures. But very often, those results are not reported at iso-CH_4 conversion, in which case no conclusions can actually be drawn about what phenomena are taking place. Other works report a decrease in C_2 selectivity at higher temperatures, without reporting the stability of their catalyst at those higher temperatures. Still others, report the C_2 selectivity versus temperature using the furnace temperature on the x-axis, which may significantly differ from the actual temperature in the reactor (this comment basically applies to the whole OCM experimental literature). It should also be mentioned that a lot of confusion is probably created by the fact that the famous Stansch model [15] explicitly contains a reforming reaction that will cause the C_2 selectivity to drop at high temperatures.

SI-3. VALIDATION STUDY

Since large parts of the code, especially everything related to the chemistry in the solid phase, were implemented in catchyFOAM from scratch, a proper validation is needed. In order to validate the implementation of the kinetics and the two-phase reactive framework described in §2 of the paper, 1D simulations of a packed bed reactor are performed. The boundary conditions and simulation settings are chosen such as to resemble ideal plug flow behavior as close as possible. This allows a comparison with Cantera simulations of a 1D pseudo-homogeneous plug flow reactor.
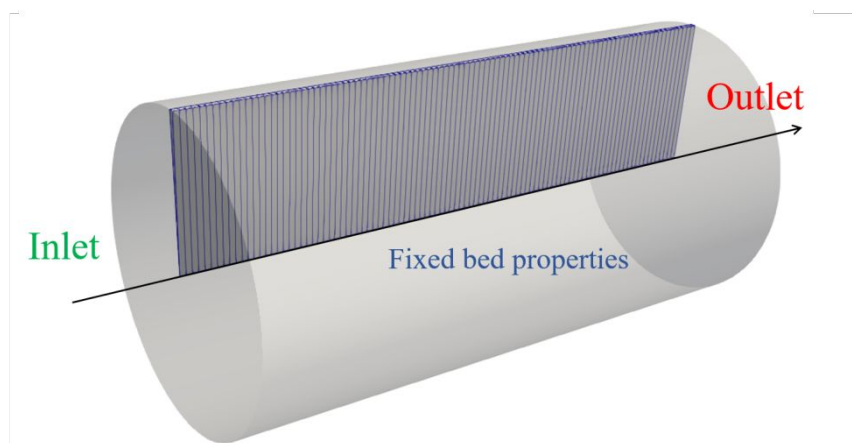

Figure SI 2: Geometry and computational grid used for the validation study.

The geometry and computational grid used for this validation study are shown in Figure SI 2. A cylindrical packed bed reactor is considered, which allows to use a wedge-type grid. Furthermore, only one cell is considered in the radial direction, turning this validation case into a 1D problem. The computational domain is discretized in 500 cells in the axial direction. For the spatial discretization a second-order upwind scheme is employed. The time is discretized using the implicit first-order Euler method. The solver is operated in PISO mode. The time step is dynamically adjusted to maintain a maximum Courant number of 0.5, following the CFL

condition. However, only the steady-state results are reported below. The operating conditions are summarized in Table SI 3. A laminar model is used for the gas phase, while the solid phase is modeled as a stationary phase. No drag model is used so no pressure drop over the reactor is simulated.

Table SI 3: Validation study: geometry and operating conditions.

Packed bed geometry	
Diameter	0.005 m
Length	0.010 m
Gas phase properties	
Kinetics and thermo	Stagni et al. [11]
Density	Ideal gas law
Solid phase properties	
Kinetics	4%Sr-40%La/SiC (see §SI-1)
Density	2950 kg m^{-3}
Diameter	500 μm
Specific heat capacity	5 J kg^{-1} K^{-1}
Volume fraction	0.55
Porosity	0.27
Catalytic surface area per volume, $a_{c,V}$	18.29 10^6 m$_c^2$ m$_s^{-3}$
Boundary conditions	
Inlet composition	CH_4:O_2:N_2 = 4:1:0 (isothermal)
	CH_4:O_2:N_2 = 4:1:20 (adiabatic)
Inlet temperature	1423 K (gas-only isothermal)
	1098 K (isothermal)
	973 K (adiabatic)
Inlet velocity	2.5 m s^{-1} (isothermal)
	5.0 m s^{-1} (adiabatic)
Outlet pressure	1.1 bar

Several cases are considered, in which the complexity of the model is gradually increased to validate all parts of the code.

SI-3.1. *ISOTHERMAL, ONLY GAS PHASE CHEMISTRY*

In the simplest case, the chemistry in the solid phase is disabled ($\tilde{R}_{s,k} = 0$) so only reactions in the gas phase are accounted for, and this under isothermal conditions at 1423 K. Figure SI 3 shows the resulting mass fractions of the reactants and the most relevant products as a function of axial coordinate. A perfect agreement is obtained between the OpenFOAM results (dashed lines) and the results of a PFR simulation in Cantera (full lines). This is not surprising because, apart from the conversion of the input format, only default OpenFOAM features were needed for this gas-only simulation.

(a)   (b)
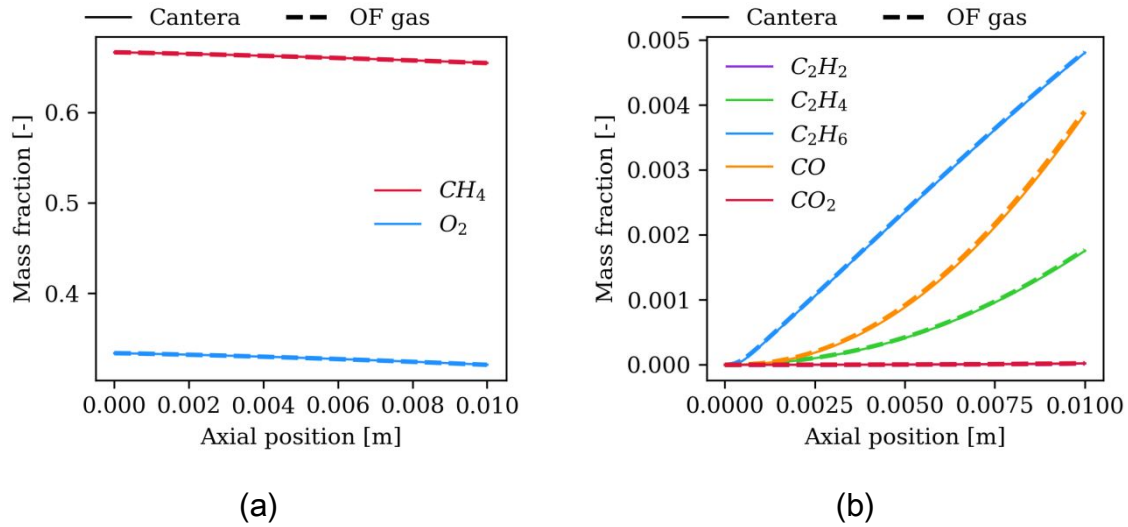
Figure SI 3: Isothermal, gas-only case. OF results when only gas phase chemistry is enabled, and comparison with PFR simulation in Cantera: (a) reactant mass fractions, and (b) product mass fractions as a function of axial coordinate. Operating conditions: see Table SI 3.

When mass transfer limitations are neglected, i.e., when using eqn. (24), a further reduction of the computational cost is possible by numerically disabling the chemistry in the gas phase, so that $\tilde{R}_{g,k} = 0$, and meanwhile substituting

$$\overrightarrow{R_s}\left(\overrightarrow{C_s}, T_s, p\right) = \begin{bmatrix} a_{c,V}R_{c,1}\left(\overrightarrow{C_s}, T_s, p\right) + \left(\varepsilon_p + \dfrac{\varepsilon_g}{\varepsilon_s}\right)R_{g,1}\left(\overrightarrow{C_s}, T_s, p\right) \\ \vdots \\ a_{c,V}R_{c,n_g}\left(\overrightarrow{C_s}, T_s, p\right) + \left(\varepsilon_p + \dfrac{\varepsilon_g}{\varepsilon_s}\right)R_{g,n_g}\left(\overrightarrow{C_s}, T_s, p\right) \\ R_{c,\theta,1}\left(\overrightarrow{C_s}, T_s, p\right) \\ \vdots \\ R_{c,\theta,n_s}\left(\overrightarrow{C_s}, T_s, p\right) \end{bmatrix} \qquad \text{(SI-11)}$$

in the stiff chemistry solver for the solid phase. Because the chemistry in the gas phase no longer has to be solved, the simulation time can be significantly reduced in this way. The only downside of this "coupled chemistry" methodology is that no separate generated thermal power for the gas and solid phase can be calculated via eqn. (30). In the following validation case, this coupled chemistry approach is used to model an isothermal OCM reactor at 1098 K. The resulting product mass fractions and surface coverages are shown in Figure SI 4. Because no mass transfer limitations are considered, the species mass fractions in the gas phase (dashed lines) overlap with those in the solid phase (dotted lines). A perfect agreement with a pseudo-homogeneous PFR simulation in Cantera is obtained for all variables (full lines). Although not shown in the figure, a perfect agreement was also observed for CH_4 and O_2.
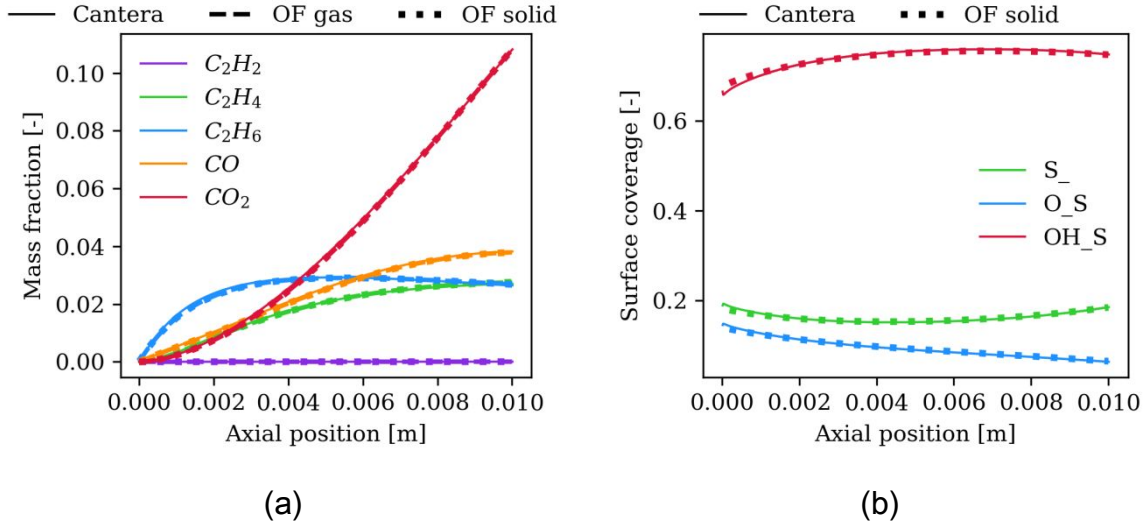
Figure SI 4: Isothermal, gas-solid case. OF results with the coupled chemistry approach and without considering mass transfer limitations, and comparison with PFR simulation in Cantera: (a) product mass fractions, and (b) surface coverages as a function of axial coordinate. Operating conditions: see Table SI 3.

The above two cases show that the implementation of the chemistry and calculation of the reaction rates in both separate phases is correct. Also, the implementation of eqn. (24) when mass transfer limitations are neglected, is working as intended.

SI-3.3. *ISOTHERMAL, SEGREGATED GAS AND SOLID PHASE CHEMISTRY, NO MASS TRANSFER LIMITATIONS*

The next case considers the segregated chemistry approach where the chemistry is solved in both the gas and the solid phase. Mass transfer limitations are still neglected. Figure SI 5 shows that, with these settings, although the difference is minor, there is no longer a perfect agreement between the OpenFOAM results and Cantera results. This is somehow surprising since the previous two cases indicated that all individual parts of the model are implemented correctly.

15

The reason for the discrepancies is the use of separate stiff chemistry solvers for the gas and solid phase. As such, when also neglecting mass transfer limitations and substituting eqn. (24) in eqn. (7), the total chemical source term vector becomes:

$$\varepsilon_g \overrightarrow{\widetilde{R_g}} + \varepsilon_s \overrightarrow{\widetilde{R_s}} = \frac{\varepsilon_g}{\Delta t} \int_t^{t+\Delta t} \overrightarrow{R_g}\big(\overrightarrow{C_g}(t), T_g, p\big) dt + \frac{\varepsilon_s}{\Delta t} \int_t^{t+\Delta t} \overrightarrow{R_s}\big(\overrightarrow{C_s}(t), T_s, p\big) dt \qquad \text{(SI-12)}$$

This is not equal to the following expression:

$$\frac{1}{\Delta t} \int_t^{t+\Delta t} \Big[\varepsilon_g \overrightarrow{R_g}\big(\overrightarrow{C_s}(t), T_s, p\big) + \varepsilon_s \overrightarrow{R_s}\big(\overrightarrow{C_s}(t), T_s, p\big)\Big] dt \qquad \text{(SI-13)}$$

which would be the result when using eqn. (SI-11) as was done in validation case 2, and which also corresponds to the assumptions made in the pseudo-homogeneous PFR model. By reducing the computational time step Δt, the integrated reaction rates approach the instantaneous reaction rates. Hence, the difference between eqn. (SI-12) and (SI-13) becomes smaller and the OpenFOAM results approach the Cantera results.

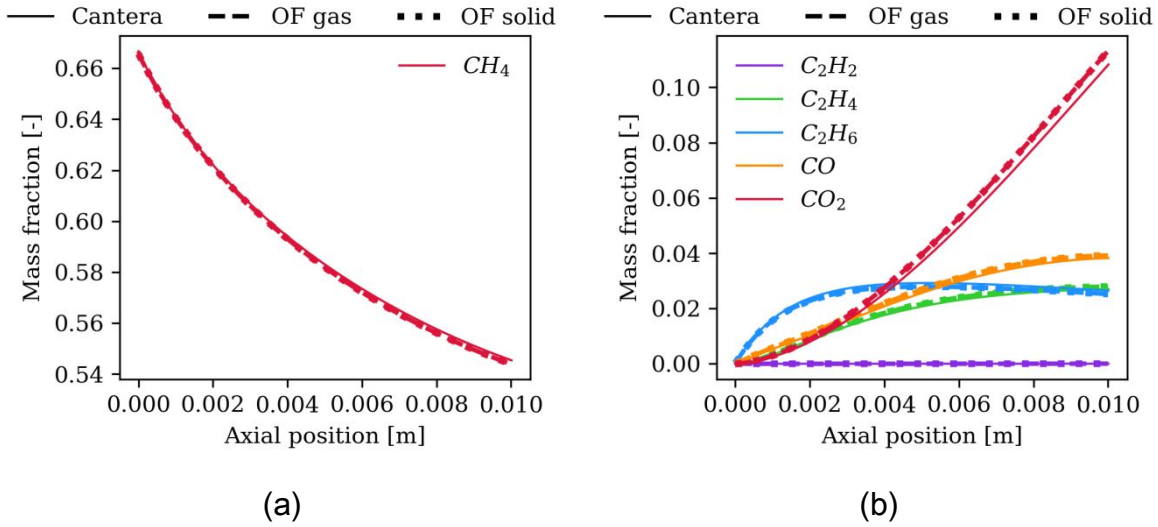(a)   (b)

Figure SI 5: Isothermal, gas-solid case. OF results with the segregated chemistry approach and without considering mass transfer limitations, and comparison with PFR simulation in Cantera: (a) reactant mass fractions, and (b) product mass fractions as a function of axial coordinate. Operating conditions: see Table SI 3.

SI-3.4. ISOTHERMAL, SEGREGATED GAS AND SOLID PHASE CHEMISTRY, INCLUDING MASS TRANSFER LIMITATIONS

In the last isothermal validation case, mass transfer limitations are no longer neglected. Eqn. (21) is used together with the correlation for the mass transfer coefficient given by eqns. (22)-(23), where Sc_g is set to 1. The segregated chemistry approach is used. The CH_4 and product mass fraction profiles are shown in Figure SI 6 for two different particle diameters. Because of the non-instantaneous mass transfer, the species mass fractions in the gas and solid phase are not the same. Both are also different from the pseudo-homogeneous result. For a smaller particle diameter, the results approach the pseudo-homogeneous model results. As can be seen in Figure SI 6, for the simulated conditions, diffusion limitations occurring for larger catalyst particle diameters result in a significant decrease in conversion and C_2 selectivity.

As discussed in by Kechagiopoulos et al. [3], mass transfer limitations during OCM are due to the high reactivity of surface-produced radicals, such as CH_3. For these radicals, the difference between the mass fraction in the solid phase and gas phase is more pronounced. However, this is not elaborated on in this part of the work.
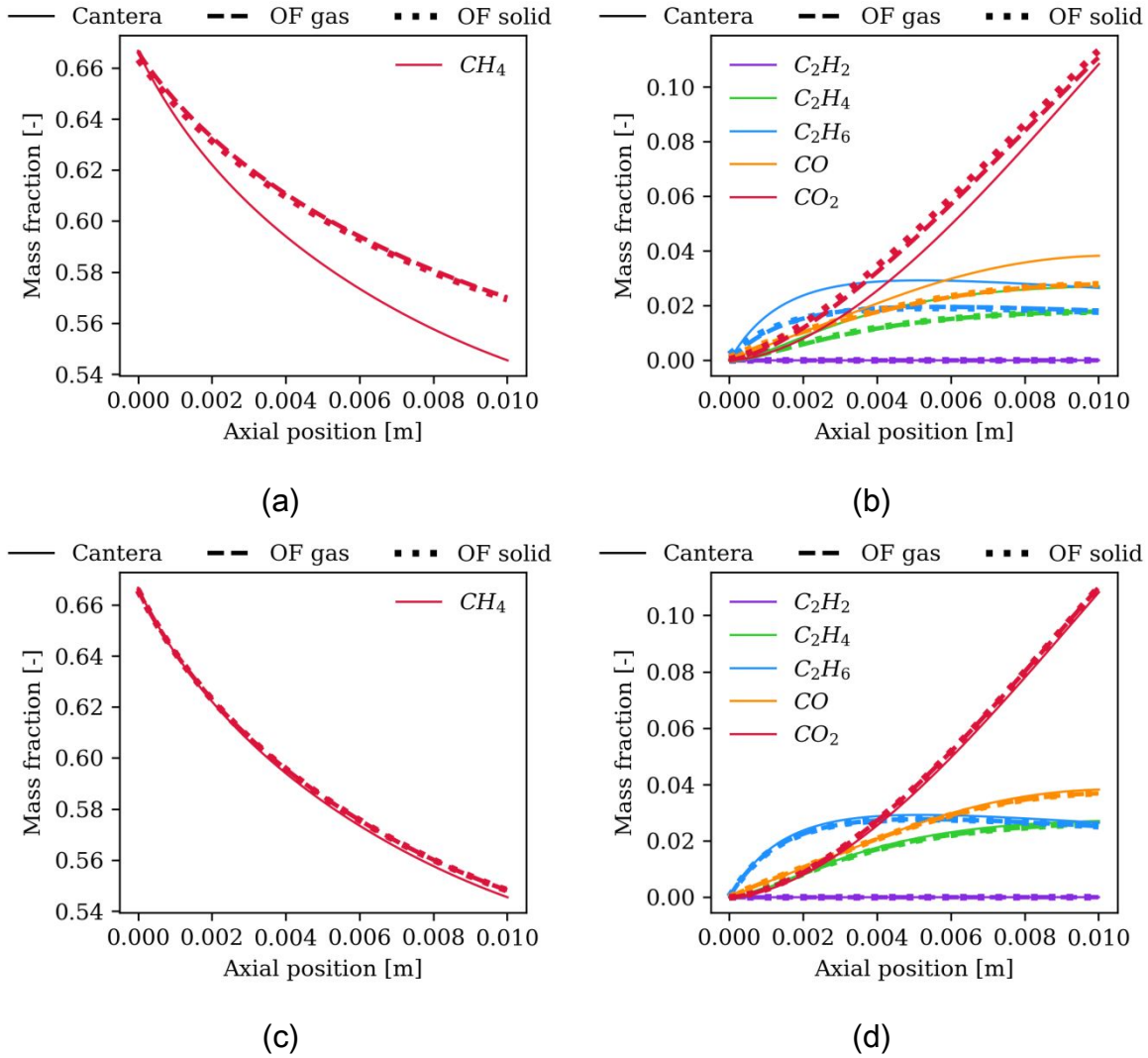
Figure SI 6: Isothermal, gas-solid case. OF results with the coupled chemistry approach and considering mass transfer limitations, and comparison with PFR simulation in Cantera: (a) CH_4 mass fraction, and (b) product mass fractions as a function of axial coordinate for d_p = 500 μm. (c) CH_4 mass fraction, and (d) product mass fractions as a function of axial coordinate for d_p = 50 μm Operating conditions: see Table SI 3.

SI-3.5. ADIABATIC, COUPLED GAS AND SOLID PHASE CHEMISTRY, NO MASS TRANSFER

LIMITATIONS

An adiabatic case is considered next. The temperature is therefore decreased to 973 K, 80 % N_2 dilution is added and the inlet velocity is increased to 5 m s^{-1}. As can be seen in Table SI 3, a very

18

low value is selected for the solid phase specific heat capacity. In the present validation study, only the steady state matters. The steady state is not influenced by the value of the solid phase heat capacity. However, the computational time required to reach this steady state can be significantly reduced by lowering the solid phase heat capacity and therefore reducing the thermal inertia of the system. A value of $5 \text{ J kg}^{-1} \text{ K}^{-1}$ is selected as it provides a reasonable tradeoff between computation time and stability.

The coupled chemistry approach is used and mass transfer limitations are neglected. As mentioned earlier, the downside of this coupled chemistry approach is that no separate reaction heat can be calculated for the gas and the solid phase, since no distinction can be made between reactions happening in the particles and reactions happening in the gas phase.

(a)   (b)

Figure SI 7: Adiabatic, gas-solid case. OF results with the coupled chemistry approach, with all heat generated in the solid phase, and without considering mass transfer limitations, and comparison with PFR simulation in Cantera: (a) CH$_4$ mass fraction, and (b) temperature as a function of axial coordinate. Operating conditions: see Table SI 3.

By default, the use of eqn. (SI-11), results in all reaction heat being produced in the solid phase. The resulting temperature and CH$_4$ mass fraction profiles are shown in Figure SI 7. Two observations can be made: 1) the simulated gas temperature is lower than the solid temperature,

and 2) both of them are overestimating the PFR result from Cantera. Because of the higher temperatures, the CH$_4$ conversion is also overestimated with the OpenFOAM model. At first, one may think that this indicates an erroneous implementation in the code. However, the results can be explained by looking at the energy balance, eqn. (11)-(12) in the main paper. Neglecting the thermal diffusion and potential energy terms, and assuming steady state, the energy balance for both phases can be integrated over a control volume between two axial positions z_1 and z_2, yielding the following balances:

$$\dot{H}_{g,z_2} - \dot{H}_{g,z_1} = h\frac{6\varepsilon_s}{d_s}(\overline{T}_s - \overline{T}_g) + \varepsilon_g Q_{r,g}|_{z_1 - z_2} \tag{SI-14}$$

$$0 = h\frac{6\varepsilon_s}{d_s}(\overline{T}_g - \overline{T}_s) + \varepsilon_s Q_{r,s}|_{z_1 - z_2} \tag{SI-15}$$

where $\overline{T}_g$ and $\overline{T}_s$ are the volume-weighted average gas and solid temperatures in the control volume, and $Q_g|_{z_1 - z_2}$ and $Q_s|_{z_1 - z_2}$ are the total reaction heat generated in the control volume in the gas and the solid phase, respectively. Eqn. (SI-15) shows that, for any case where the reaction heat in the solid phase is non-zero, there will always be a finite difference between the gas phase temperature and the solid-phase temperature. When all the reaction heat is produced in the solid phase, i.e., when $Q_g|_{z_1 - z_2}$ is added in eqn. (SI-15), the difference in temperature between the gas and the solid phase is overestimated. Substituting eqn. (SI-15) into eqn. (SI-14) shows that this should not make a difference for the gas phase temperature. However, an overestimation of the solid temperature, at which reaction rates are calculated, results in an overestimation of the reaction heat, and this does influence the gas phase temperature. A steady state is therefore obtained at higher temperatures than the one resulting from a pseudo-homogeneous adiabatic PFR simulation.

In order to approximate the pseudo-homogeneous adiabatic PFR simulation, it can be forced that all reaction heat ends up in the gas phase. As shown in Figure SI 8, under this assumption, a perfect

agreement between the OpenFOAM results and Cantera results is obtained. This proves that the calculation of reaction heats and heat transfer in the code is done correctly.
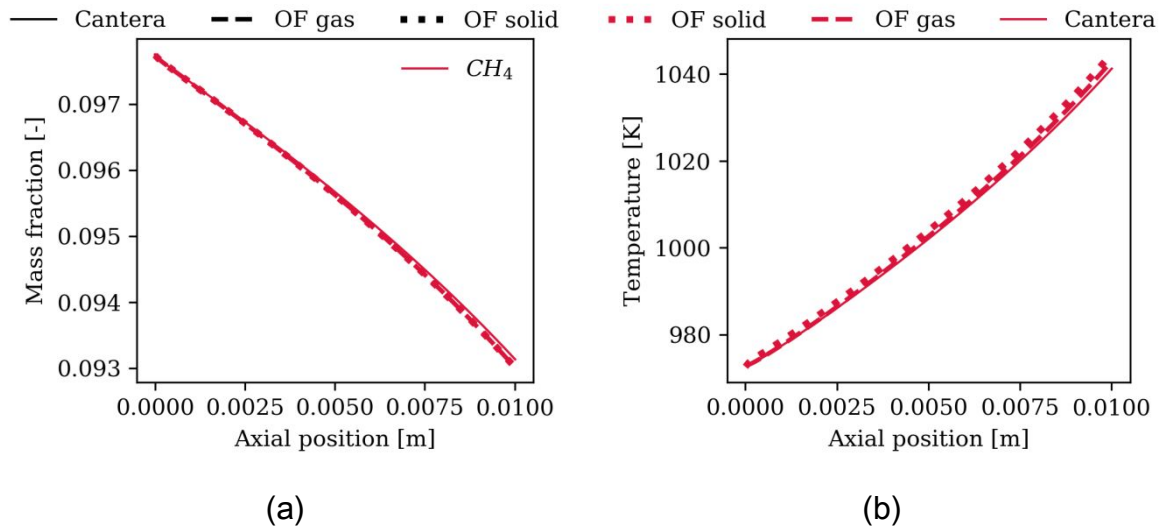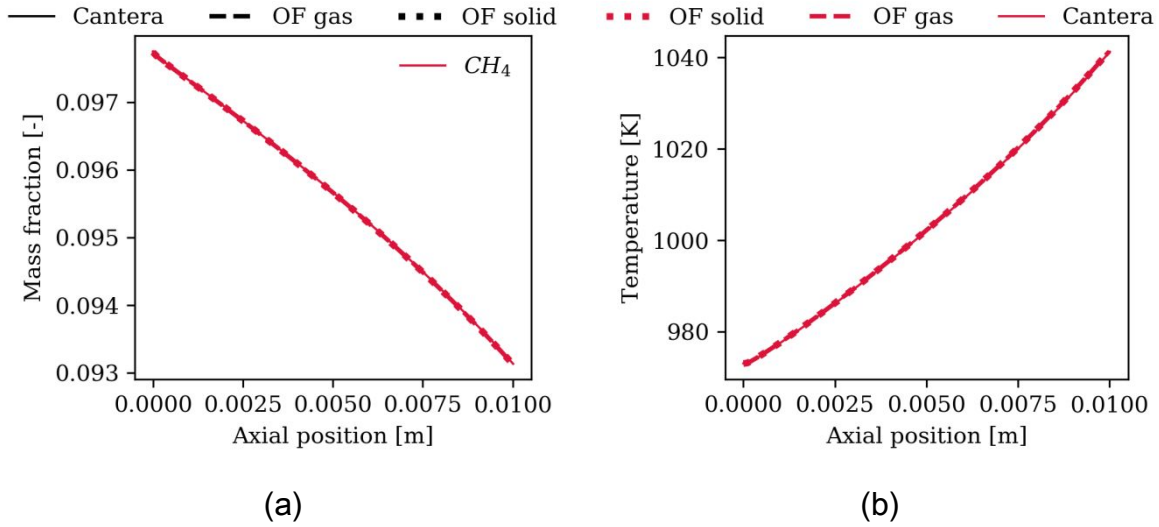

Figure SI 8: Adiabatic, gas-solid case. OF results with the coupled chemistry approach, with all heat generated in the gas phase, and without considering mass transfer limitations, and comparison with PFR simulation in Cantera: (a) CH$_4$ mass fraction, and (b) temperature as a function of axial coordinate. Operating conditions: see Table SI 3.

It should be noted that the results from the PFR simulation in Figure SI 7 and Figure SI 8 don't reflect the situation in an actual packed bed. As explained above, the finite difference between the gas and solid phase temperatures has an effect on the reaction heat produced in the solid phase. For the OpenFOAM results in Figure SI 7, this effect is overestimated, while for Figure SI 8 it is ignored. Hence, the situation in an actual packed bed will be somewhere in between the OpenFOAM results from Figure SI 7 and Figure SI 8.

Finally, the same adiabatic case is simulated including mass transfer limitations and with segregated chemistry solvers for the two phases. Having validated all separate parts of the code in cases 1-5, it is safe to assume that the OpenFOAM results in Figure SI 9 reflect a possible situation in an actual bed. *That is, if the applied heat and mass transfer correlations are valid.* The difference with the Cantera simulations are simply due to the fact that the pseudo-homogeneous PFR model doesn't take into account heat and mass transfer limitations while both are included in the OpenFOAM model.
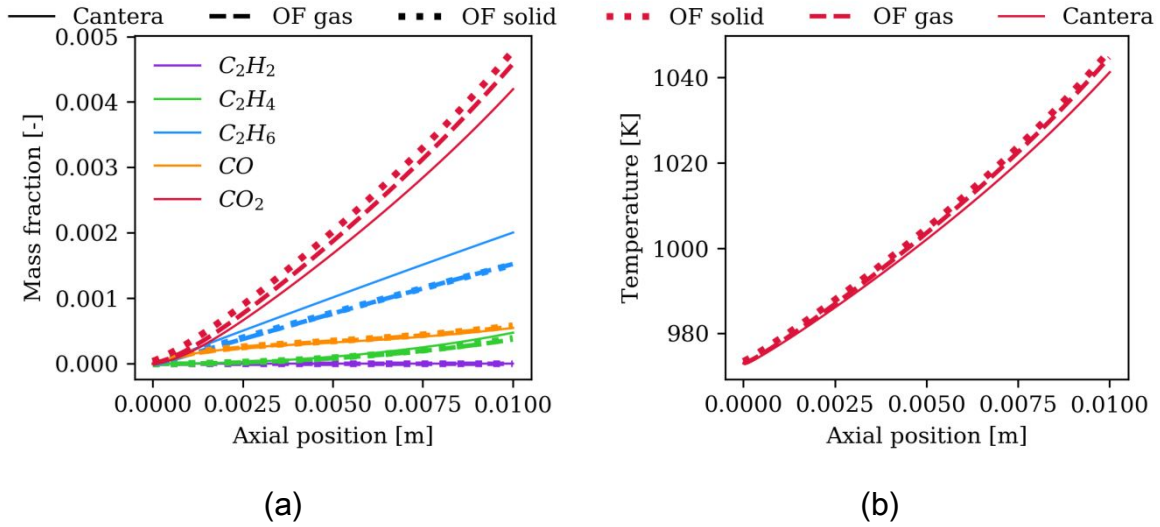
Figure SI 9: Adiabatic, gas-solid case. OF results with the segregated chemistry approach, considering both heat and mass transfer limitations, and comparison with PFR simulation in Cantera: (a) product mass fractions and (b) temperature as a function of axial coordinate. Operating conditions: see Table SI 3.

Based on the validation cases presented above, it can be concluded that the chemistry implementation works as intended. For the simulations of OCM in the GSVR, the segregated chemistry approach is used, without considering mass transfer limitations.

SI-4. TUTORIALS ON GITHUB

Tutorials for the multiphaseEulerFoam solver with catchyFOAM are available on the catchyFOAM github page:

https://github.com/lavdwall/catchyFOAM/tree/openfoam8/tutorials/catchyMultiphaseEulerFoam

An overview of the available tutorials is given below. It should be stresses that these tutorials are not exactly the same as the cases discussed in the manuscript. For examples, the following items are different (amongst others):

- Kinetic model: due to confidentiality, the catalytic kinetic mechanism could not be shared in Cantera or OpenFOAM format. A similar mechanism was used, corresponding to the 1%Sr/La$_2$O$_3$ catalyst in Table SI 2. Because of this difference in kinetics, the results obtained in the tutorials cannot be directly compared to the results in the manuscript.

- Discretization schemes: first-order spatial discretization schemes are used in the tutorials, to guarantee stability when running them.

- Transport / thermo model: the Sutherland transport model is used in some tutorials instead of the logPolynomial transport model.

- The grid of the packed bed validation cases is coarser in the tutorials

The user is free to adjust these settings in case necessary.

SI-4.1. PACKED BED VALIDATION CASES

The following tutorials, similar (but not identical) to the packed bed validation cases discussed in the manuscript, are available.

23

isothermalGasonly Isothermal 1D packed bed reactor with inert particles. Only gas phase reactions are considered (chemistry is disabled in *chemistryProperties.particles*).

isothermalCoupled Isothermal 1D packed bed reactor with reactions in both the gas phase and particles phase. The coupled chemistry approach is used, by disabling the chemistry in *chemistryProperties.gas* and using the 'twoPhaseAlpha' option in *chemistryProperties.particles*. No mass transfer resistances are considered.

isothermalSegregated Isothermal 1D packed bed reactor with reactions in both the gas phase and particles phase. The segregated chemistry approach is used. No mass transfer resistances are considered.

isothermalSegregatedMassTransfer Isothermal 1D packed bed reactor with reactions in both the gas phase and particles phase. The segregated chemistry approach is used. Mass transfer is modeled using a film model with mass transfer coefficient from an analogy with the Gunn correlation for heat transfer.

adiabaticCoupledSolidheat Adiabatic 1D packed bed reactor with reactions in both the gas phase and particles phase. The coupled chemistry approach is used. No mass transfer resistances are considered. All reaction heat is generated in the particles phase.

adiabaticCoupledGasheat Adiabatic 1D packed bed reactor with reactions in both the gas phase and particles phase. The coupled chemistry approach is used. No mass transfer resistances are considered. All reaction heat is forced to be generated in the gas phase, by enabling the 'multiphaseReactionHeat' option (default: off) in the *reactiveGasExchange* dictionary in *phaseProperties*.

adiabaticSegregatedMassTransfer Adiabatic 1D packed bed reactor with reactions in both the gas phase and particles phase. The segregated chemistry approach is used. Mass transfer is modeled using a film model with mass transfer coefficient from an analogy with the Gunn correlation for heat transfer.

This information, as well as instructions on how to run the cases, is also available in the README file on Github.

SI-4.2. GAS-SOLID VORTEX REACTOR

A GSVR tutorial, with a similar (but not identical) setup than the simulations discussed in the manuscript, is also provided. The following information is also available in the accompanying README file:

> This tutorial considers a 2D isothermal simulation of a GSVR with 16 inlet slots.
>
> First, the hydrodynamics are calculated while the chemistry is still disabled. The solids are fed in a ring shaped volume near the circumferential wall of the reactor chamber (defined in *system/topoSetDict*). They are fed in this ring via a numerical source term, as specified in *constant/fvOptions*. A residence time distribution is constructed by solving a scalar transport equation for tau.gas (using the 'phaseScalarTransport' functionObject).
>
> Next, the OCM chemistry is enabled. The segregated chemistry approach is used. Mass transfer is modeled using a film model with mass transfer coefficient from an analogy with the Gunn correlation for heat transfer.
>
> For convenience, the most important case settings in terms of operating conditions are bundled in *system/caseSettings* and should only be adjusted by the user in that file.

SI-5. CHEMISTRY / THERMO INPUT FILES

Example input files to specify the catalytic solid phase in catchyFOAM are shown below. These are very similar to the classical thermophysicalProperties and chemistryProperties files in OpenFOAM, with a few distinct differences.

In **thermophysicalProperties.<phaseName>**, the thermo for both the (internal) gas phase and the solid phase itself has to be provided, via the keywords gasThermoType and solidThermoType. The thermo/transport of the internal gas phase is hereby only needed when calculating the mass transfer coefficients and reaction heat. The solid-phase thermo/transport is used when solving the hydrodynamics.

```
/*--------------------------------*- C++ -*----------------------------------*\
  =========                 |
  \\      /  F ield          | OpenFOAM: The Open Source CFD Toolbox
   \\    /   O peration      | Website:  https://openfoam.org
    \\  /    A nd            | Version:  8
     \\/     M anipulation   |
\*---------------------------------------------------------------------------*/
FoamFile
{
    version     2.0;
    format      ascii;
    class       dictionary;
    location    "constant";
    object      thermophysicalProperties.particles;
}
// * * * * * * * * * * * * * * * * * * * * * * * * * * * * * * * * * * * * * //

gasThermoType
{
    type            heRhoThermo;
    mixture         multiComponentMixture;
    transport       logPolynomial;
    thermo          janaf;
    energy          sensibleEnthalpy;
    equationOfState perfectGas;
    specie          specie;
}

solidThermoType
{
    type            heRhoThermo;
    mixture         multiComponentGSMixture;
    transport       const;
    thermo          hConst;
    equationOfState rhoConst;
```

```
    specie           specie;
    energy           sensibleEnthalpy;
}

pressureWorkAlphaLimit  1;

#include "mechanism/thermo.catalyst"

// ************************************************************************* //
```

For a multiComponentGSMixture, the properties of the individual species are provided in a separate file (**mechanism/thermo.catalyst**, which is provided below), where again a distinction is made between internal gas and solid. The gas thermo is the same as the one used for the actual gas phase (in below example provided in **thermo.gas**). The surface thermo is provided in **thermo.surf**. The **thermo.gas** and **thermo.surf** files can be manually constructed, or the *canteraToFoam* utility can be used to automatically create these files from a cantera input mechanism file. Note that the names of these files are arbitrary and can be changed when the corresponding #include statements are adjusted.

```
/*--------------------------------*- C++ -*----------------------------------*\
  =========                 |
  \\      /  F ield          | OpenFOAM: The Open Source CFD Toolbox
   \\    /   O peration       | Website:  https://openfoam.org
    \\  /    A nd            | Version:  8
     \\/     M anipulation   |
\*---------------------------------------------------------------------------*/
FoamFile
{
    version     2.0;
    format      ascii;
    class       dictionary;
    location    "mechanism";
    object      thermo.catalyst;
}
// * * * * * * * * * * * * * * * * * * * * * * * * * * * * * * * * * * * * * //

gas
{
    #include "thermo.gas"
}

solid
{
    #include "thermo.surf"
}

// ************************************************************************* //
```

```
// thermo.surf

species
11
(
_S_
O_S
OH_S
H2O_S
CH3O_S
CH2O_S
CHO_S
CO_S
CO2_S
C2H3O_S
C2H4O_S
)
;


CO_S
{
    specie
    {
        molWeight       100;
        size            1;
        surfaceDensity  9.84e-09;
    }
    equationOfState
    {
        rho             2950;
    }
    thermodynamics
    {
        Cp              5;
        Hf              0;
        Cv              5;
    }
    transport
    {
        mu              0;
        Pr              1;
    }
}

…
```

Information about the kinetics is given in **chemistryProperties.< phaseName >.** Here, general

properties of the catalyst are specified, such as the porosity and the surface-area-to-volume ratio.

There is an option to initialize the coverages using the QSSA. The twoPhaseAlpha keyword is a

switch to turn on the coupled chemistry approach. It is also possible to disable the solution of the

chemistry in the solid phase (both catalytic and internal gas phase) when the volume fraction is

lower than the specified alphaMin. The reactions are specified in a separate file (**mechanism/reactions.catalyst**, which is provided below). There a distinction is again made between the gas and solid chemistry. The reaction input files **chem.gas** and **chem.surf** can be manually constructed, or the *canteraToFoam* utility can be used to automatically create these files from a cantera input mechanism file.

```
/*--------------------------------*- C++ -*----------------------------------*\
  =========                 |
  \\      /  F ield          | OpenFOAM: The Open Source CFD Toolbox
   \\    /   O peration       | Website:  https://openfoam.org
    \\  /    A nd             | Version:  8
     \\/     M anipulation   |
\*---------------------------------------------------------------------------*/
FoamFile
{
    version     2.0;
    format      ascii;
    class       dictionary;
    location    "constant";
    object      chemistryProperties.particles;
}
// * * * * * * * * * * * * * * * * * * * * * * * * * * * * * * * * * * * * * //

catalystPorosity                0.27;
catalyticSurfaceAreaPerVolume   5.9e6;
alphaMin                        0.0;
twoPhaseAlpha                   false;

initializeCoveragesQSSA         true;
coveragesQSSA
{
    deltaT                      1e-3;
    uniformCoverages            true;
}

#include "mechanism/reactions.catalyst"

// ---------------------------------------------------------------------------//

chemistryType
{
    method          gsPhase;
    solver          gsOde;
}

chemistry           on;

initialChemicalTimeStep 1e-07;

odeCoeffs
{
    solver          seulex;
    absTol          1e-8;
```

```
    relTol          0.01;
}


// ********************************************************************* //
```

```
/*--------------------------------*- C++ -*----------------------------------*\
  =========                 |
  \\      /  F ield          | OpenFOAM: The Open Source CFD Toolbox
   \\    /   O peration      | Website:  https://openfoam.org
    \\  /    A nd            | Version:  8
     \\/     M anipulation   |
\*---------------------------------------------------------------------------*/
FoamFile
{
    version     2.0;
    format      ascii;
    class       dictionary;
    location    "mechanism";
    object      reactions.catalyst;
}
// * * * * * * * * * * * * * * * * * * * * * * * * * * * * * * * * * * * * * //

gas
{
    #include "chem.gas"
}

solid
{
    gasesThermoLocation "$FOAM_CASE/constant/mechanism/thermo.catalyst";
    #include "chem.surf"
}

// ********************************************************************* //
```

```
// chem.surf

reactions
{
    un-named-reaction-0
    {
        type            irreversibleSurfaceArrhenius;
        reaction        "2_S_ + O2 = 2O_S";
        A               3.719e+16;
        beta            0.5;
        Ta              0;
    }
    un-named-reaction-1
    {
        type            irreversibleSurfaceArrhenius;
        reaction        "2O_S = 2_S_ + O2";
        A               2.39e+20;
        beta            0;
        Ta              13590.77612;
    }

…
```

REFERENCES

[1]   C.R. Wilke, A Viscosity Equation for Gas Mixtures, J. Chem. Phys. 18 (1950) 517–519. https://doi.org/10.1063/1.1747673.

[2]   J. Sun, J. Thybaut, G. Marin, Microkinetics of methane oxidative coupling, Catal. Today. 137 (2008) 90–102. https://doi.org/10.1016/j.cattod.2008.02.026.

[3]   P.N. Kechagiopoulos, J.W. Thybaut, G.B. Marin, Oxidative Coupling of Methane: A Microkinetic Model Accounting for Intraparticle Surface-Intermediates Concentration Profiles, Ind. Eng. Chem. Res. 53 (2014) 1825–1840. https://doi.org/10.1021/ie403160s.

[4]   V.I. Alexiadis, J.W. Thybaut, P.N. Kechagiopoulos, M. Chaar, A.C. Van Veen, M. Mühler, G.B. Marin, Oxidative coupling of methane: catalytic behaviour assessment via comprehensive microkinetic modelling, Appl. Catal. B Environ. 150–151 (2014) 496–505. https://doi.org/10.1016/j.apcatb.2013.12.043.

[5]   V.I. Alexiadis, M. Chaar, A. van Veen, M. Muhler, J.W. Thybaut, G.B. Marin, Quantitative screening of an extended oxidative coupling of methane catalyst library, Appl. Catal. B Environ. 199 (2016) 252–259. https://doi.org/10.1016/j.apcatb.2016.06.019.

[6]   J.A. Dumesic, G.W. Huber, M. Boudart, Rates of Catalytic Reactions, in: G. Ertl, F. Schüth, J. Weitkamp (Eds.), Handb. Heterog. Catal. , Wiley-VCH, 2008: pp. 1445–1462.

[7]   J.A. Dumesic, The microkinetics of heterogeneous catalysis, An American Chemical Society Publication, 1993.

[8]   O.V. Krylov, Catalytic reactions of partial methane oxidation, Catal. Today. 18 (1993) 209–302. https://doi.org/10.1016/0920-5861(93)87001-U.

[9]   V.I. Alexiadis, T. Serres, G.B. Marin, C. Mirodatos, J.W. Thybaut, Y. Schuurman, Analysis of volume-to-surface ratio effects on methane oxidative coupling using microkinetic modeling, AIChE J. 64 (2018) 2603–2611. https://doi.org/10.1002/aic.16152.

[10]   Q. Chen, P.M. Couwenberg, G.B. Marin, Effect of pressure on the oxidative coupling of methane in the absence of catalyst, AIChE J. 40 (1994) 521–535.

[11] A. Stagni, Y. Song, L.A. Vandewalle, K.M. Van Geem, G.B. Marin, O. Herbinet, F. Battin-Leclerc, T. Faravelli, The role of chemistry in the oscillating combustion of hydrocarbons: an experimental and theoretical study, Chem. Eng. J. 385 (2020) 123401. https://doi.org/10.1016/J.CEJ.2019.123401.

[12] D. Schweer, L. Meeczko, M. Baerns, OCM in a fixed-bed reactor: limits and perspectives, Catal. Today. 21 (1994) 357–369. https://doi.org/https://doi.org/10.1016/0920-5861(94)80157-6.

[13] V.I. Lomonosov, M.Y. Sinev, Oxidative coupling of methane: Mechanism and kinetics, Kinet. Catal. 57 (2016) 647–676. https://doi.org/10.1134/S0023158416050128.

[14] S. Sarsani, D. West, W. Liang, V. Balakotaiah, Autothermal oxidative coupling of methane with ambient feed temperature, Chem. Eng. J. 328 (2017) 484–496. https://doi.org/10.1016/j.cej.2017.07.002.

[15] Z. Stansch, L. Mleczko, M. Baerns, Comprehensive Kinetics of Oxidative Coupling of Methane over the La2O3/CaO Catalyst, Ind. Eng. Chem. Res. 36 (1997) 2568–2579.